Electronic Supplementary Material (ESI) for Journal of Materials Chemistry A.

Electronic Supplementary Information for

Low Pressure Induced Porous Nanorods of Ceria with High Reducibility and Large Oxygen Storage Capacity: Synthesis and Catalytic Applications

Jing Li,[a] Zhiyun Zhang,[a] Zhimin Tian,[a] Xuemei Zhou,[a] Zhiping Zheng,[a, b,c] Yuanyuan Ma[a, b] and Yongquan Qu[a, b]*

[a]*Center for Applied Chemical Research, Frontier Institute of Science and Technology, Xi'an Jiaotong University, Xi'an, 710049, China*

Email: *yongquan@mail.xjtu.edu.cn*

[b]*Institute of Chemistry for New Energy Materials, Xi'an Jiaotong University, Xi'an, 710049, China*

[c]*Department of Chemistry and Biochemistry, University of Arizona, Tucson, Arizona 85721*

1. **Figure S1. TGA of non-porous nanorod precursor, composite of $Ce(OH)_3/CeO_2$ synthesized in a Pyrex bottle.**
2. **Figure S2. The N_2 adsorption/desorption isotherms of *PN*-Ceria-160 and *PN*-Ceria-R-160 obtained under different pressure conditions.**
3. **Figure S3. XRD spectra of the milky products after mixing $Ce(NO_3)_3$ and NaOH.**
4. **Figure S4. Characterization of the rod-shaped $Ce(OH)_3/CeO_2$ precursor obtained under 1.0 atm and the resulting nanoporous CeO_2 rods upon hydrothermal dehydration of the precursor. a,** XRD patterns of $Ce(OH)_3/CeO_2$ precursor and corresponding nanoporous CeO_2 rods. **b**, TGA of $Ce(OH)_3/CeO_2$ precursor obtained under 1.0 atm. **c**, TEM image of the $Ce(OH)_3/CeO_2$ precursor obtained hydrothermally under 1.0 atm. **d**, TEM image of the porous nanorods of ceria upon dehydration of the precursor shown in **c**.
5. **Figure S5. Plot of the surface area of ceria nanorods vs. weight percentage of**

$Ce(OH)_3$ in the three different $Ce(OH)_3/CeO_2$ precursors prior to their dehydration and subsequent oxidation of the dehydration products.

6. **Figure S6. Structural characterization of CeO_2 nanocubes, nanooctahedra and nanoparticles:** **a**, TEM image of CeO_2 nanocubes. **b**, TEM image of CeO_2 nanooctahedra. **c**, TEM image of CeO_2 nanoparticles. **d**, XRD spectra of CeO_2 nanocubes, nanooctahedra and nanoparticles.
7. **Figure S7. XPS analysis of all nanoceria: a,** XPS detail spectra of the Ce 3d core level regions for CeO_2 nanocubes and nanooctahedra. b, Survey XPS spectra of all nanoceria.
8. **Figure S8. XPS analysis. a**, Survey XPS spectra of *PN*-CeO_2-160. **b**, Comparison of *PN*-CeO_2-160 and silicon pellet survey XPS spectra.
9. **Figure S9. Raman patterns of non-porous CeO_2 nanorods, *PN*-CeO_2-160 and *PN*-CeO_2-R-160:** **a**, Raman patterns of CeO_2 nanorods in the 150-800 cm^{-1}. **b**, Raman patterns of CeO_2 nanorods in the 450-750 cm^{-1}.
10. **Figure S10. CO oxidation performance of CeO_2 nanostructures.** **a**, CO oxidation catalyzed by *PN*-CeO_2-160, non-porous CeO_2 nanorods, and CeO_2 nanoparticles. **b**, The corresponding Arrhenius plot for the three nanoceria catalysts in **a**.
11. **Table S1. Summary of previously reported OSC values for CeO_2 and chemical-doped CeO_2 nanostructures.**

1. Figure S1 TGA of non-porous nanorod precursor, composite of $Ce(OH)_3/CeO_2$ synthesized in a Pyrex bottle.

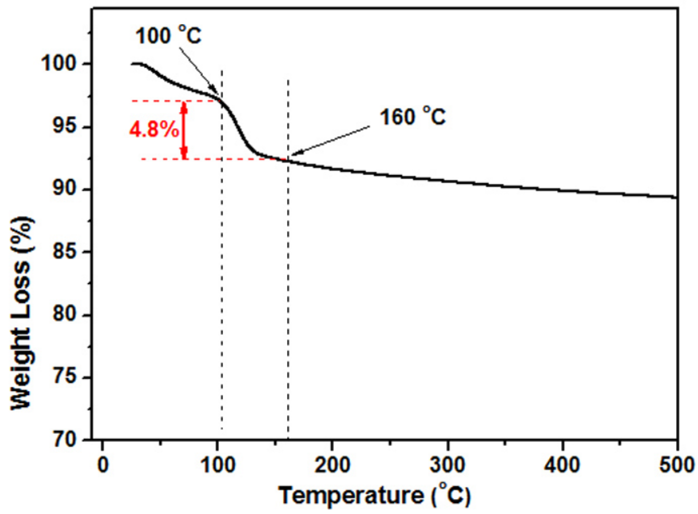

2. Figure S2 The N_2 adsorption/desorption isotherms of *PN*-Ceria-160 and *PN*-Ceria-R-160 obtained under different pressure conditions.

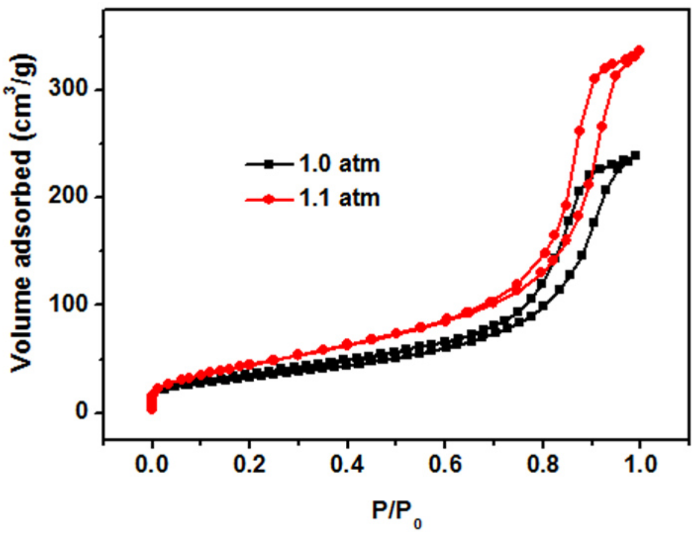

3. Figure S3 XRD spectra of the milky products after mixing $Ce(NO_3)_3$ and NaOH.

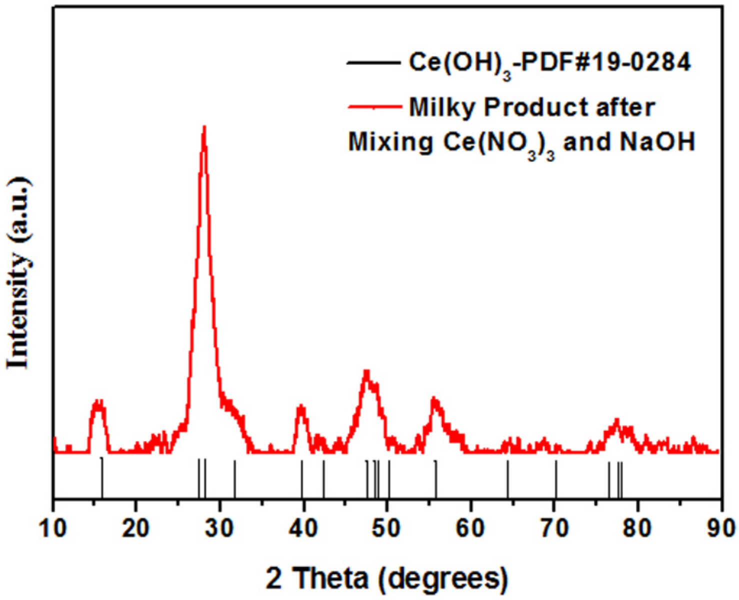

4. Figure S4 Characterization of the rod-shaped $Ce(OH)_3/CeO_2$ precursor obtained under 1.0 atm and the resulting nanoporous CeO_2 rods upon hydrothermal dehydration of the precursor. **a**, XRD patterns of $Ce(OH)_3/CeO_2$ precursor and corresponding nanoporous CeO_2 rods. **b**, TGA of $Ce(OH)_3/CeO_2$ precursor obtained under 1.0 atm. **c**, TEM image of the $Ce(OH)_3/CeO_2$ precursor obtained hydrothermally under 1.0 atm, respectively. **d**, TEM image of the porous nanorods of ceria upon dehydration of the precursors shown in **c**.

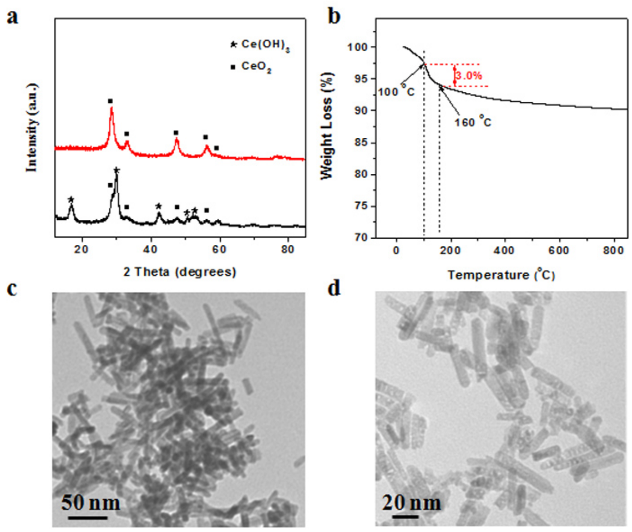

5. Figure S5 Plot of the surface area of ceria nanorods vs. weight percentage of $Ce(OH)_3$ in the three different $Ce(OH)_3/CeO_2$ precursors prior to their dehydration and subsequent oxidation of the dehydration products.

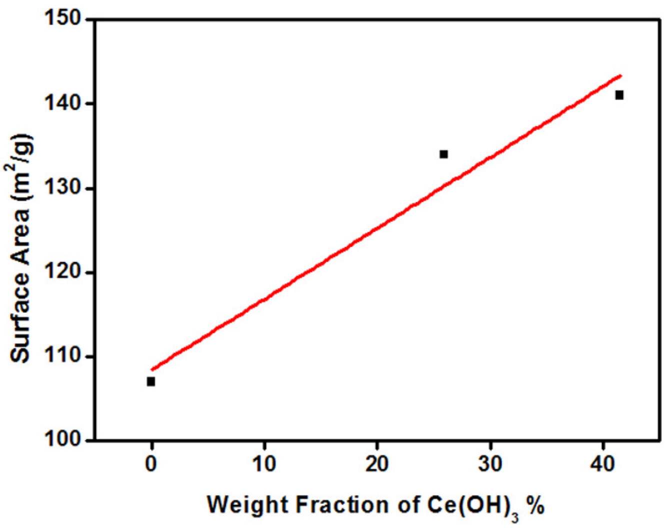

6. Figure S6 Structural characterization of CeO_2 nanocubes, nanooctahedra and nanoparticles: a, TEM image of CeO_2 nanocubes. **b**, TEM image of CeO_2 nanooctahedra. **c**, TEM image of CeO_2 nanoparticles. **d**, XRD spectra of CeO_2 nanocubes, nanooctahedra and nanoparticles.

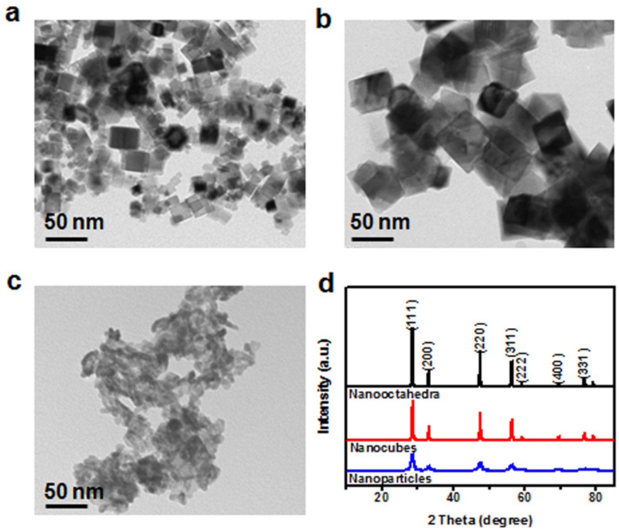

7. Figure S7 XPS analysis of all nanoceria: a, XPS detail spectra of the Ce 3d core level regions for CeO_2 nanocubes and nanooctahedra. **b**, Survey XPS spectra of all nanoceria.

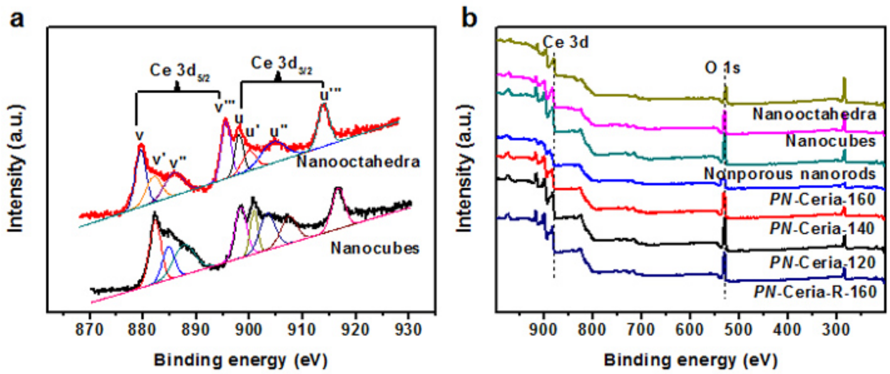

As shown in Fig. S7a, the curves of Ce 3d spectra contain eight peaks corresponding to four pairs of spin-orbit doublets. The fitting and labeling of the peaks follow the convention. Letters u and v refer to the $3d_{3/2}$ and $3d_{5/2}$ spin-obit components, respectively. The couples corresponding to one of the two possible electron configurations of the final state of the Ce^{3+} species are labeled as u' and v'. The relative percentage of the cerium species is obtained by the area ratio of Ce^{4+} $3d_{5/2}$ (v, v'' and v''')/Ce^{3+} $3d_{5/2}$ (v'). The fraction of cerium in the +3 oxidation state can is calculated from the ratio of the sum of areas of the Ce^{3+} species to the sum of areas of the total cerium species.

8. Figure S8 XPS analysis. a, Survey XPS spectra of *PN*-CeO_2-160. **b**, Comparison of *PN*-CeO_2-160 and silicon pellet survey XPS spectra.

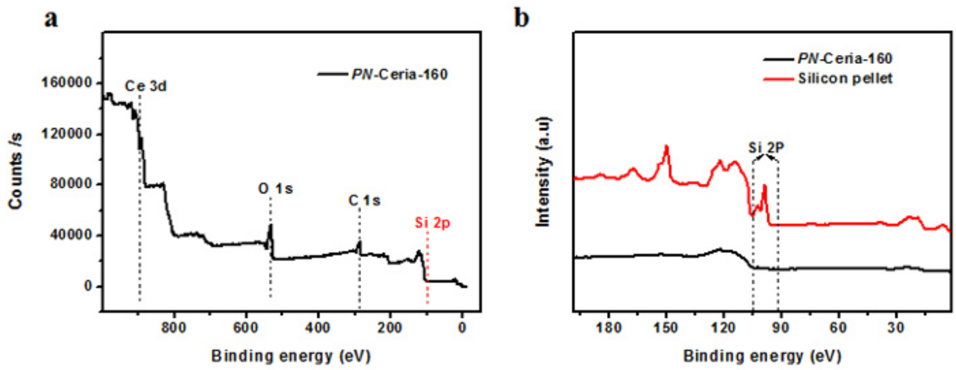

9. Figure S9 Raman patterns of non-porous CeO_2 nanorods, *PN*-CeO_2-160 and *PN*-CeO_2-R-160: a, Raman patterns of CeO_2 nanorods in the 150-800 cm^{-1}. **b**, Raman patterns of CeO_2 nanorods in the 450-750 cm^{-1}. The signal of non-porous CeO_2 nanorods was enlarged twice due to its weak intensity.

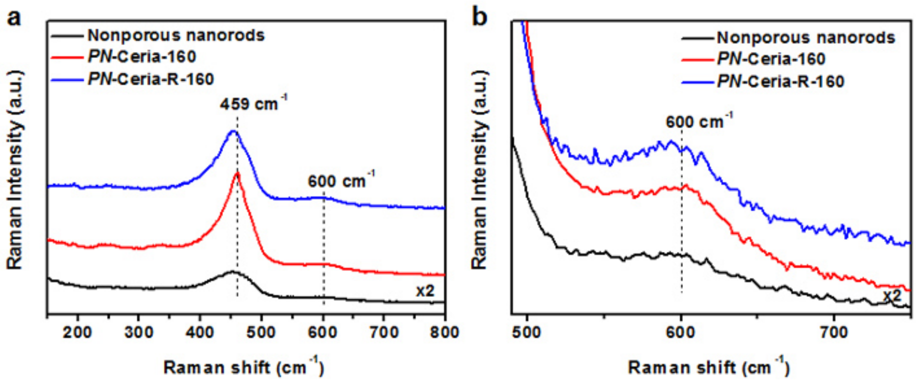

10. Figure S10 CO oxidation performance of CeO_2 nanostructures. a, CO oxidation catalyzed by *PN*-CeO_2-160, non-porous CeO_2 nanorods, and CeO_2 nanoparticles. **b**, The corresponding Arrhenius plot for the three nanoceria catalysts in **a**.

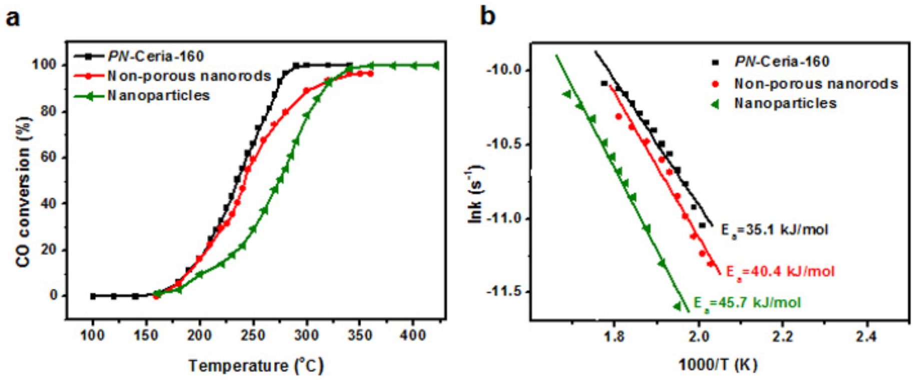

11. Table S1 Summary of previously reported OSC values for CeO_2 and chemical-doped CeO_2 nanostructures.

Table S1 Summary of previously reported OSC values for CeO_2 and chemical-doped CeO_2 nanostructures.

Sample	**BET (m^2/g)**	**OSC (μmol O_2/g)**	**Reference**
CeO_2 nanoplates	32	230.5	*1*
CeO_2 nanocrystals	61	357	*2*
CeO_2 particles	12	183	*3*
CeO_2 nanorods	60.8	277	*4*
CeO_2 particles	93	258	*5*
CeO_2-ZrO_2 particles	135	934	*5*
La-$Ce_{0.2}Zr_{0.8}O_2$ particles	144	363	*6*
Ni-$Ce_{0.67}Zr_{0.33}O_2$ particles	152	730	*7*

1. D. Wang, Y. Kang, V. Doan-Nguyen, J. Chen, R. Küngas, N. L. Wieder, K. Bakhmutsky, R. J. Gorte and C. B. Murray, *Angew. Chem. Int. Ed.*, 2011, **50**, 4378-4381.
2. J. Zhang, H. Kumagai, K. Yamamura, S. Ohara, S. Takami, A. Morikawa, H. Shinjoh, K. Kaneko, T. Adschiri and A. Suda, *Nano Lett.*, 2011, **11**, 361-364.
3. A. Gayen, K. R. Priolkar, P. R. Sarode, V. Jayaram, M. S. Hegde, G. N. Subbanna and S. Emura, *Chem. Mater.*, 2004, **16**, 2317-2328.
4. H.-X. Mai, L.-D. Sun, Y.-W. Zhang, R. Si, W. Feng, H.-P. Zhang, H.-C. Liu and C.-H. Yan, *J. Phys. Chem. B*, 2005, **109**, 24380-24385.
5. S. Letichevsky, C. A. Tellez, R. R. de Avillez, M. I. P. da Silva, M. A. Fraga and L. G. Appel, *Appl. Catal. B*, 2005, **58**, 203-210.
6. Q. Wang, G. Li, B. Zhao, M. Shen and R. Zhou, *Appl. Catal. B*, 2010, **101**, 150-159.
7. G. Li, Q. Wang, B. Zhao and R. Zhou, *Appl. Catal. B*, 2011, **105**, 151-162.